Linear Stability of the Reacting Mixing Layer

D. S. Shin* and J. H. Ferziger†
Stanford University, Stanford, California 94305

The linear instability of reacting mixing layers is analyzed with special emphasis on the effects of the heat release and variable transport properties. Both analytic profiles and laminar solutions of the boundary-layer equations are used as base flows. The growth rates of the instabilities are sensitive to the laminar profiles, differing by more than a factor of 2 according to which profile is used. Thus, it is important to base the analysis on accurate laminar profiles. Accounting for variable transport properties also changes the mean profiles considerably, and so including them in the computation of the laminar profiles is equally important. Chemical reaction that occurs during the instability hardly affects its growth rate. At larger heat release, two modes that are stronger in the outer part of the shear layer have the highest growth rates; they also have shorter wavelengths than the center mode.

I. Introduction

PREDICTION of the characteristics of chemically reacting mixing layers is very important in a number of technologies. For increased mixing, we prefer to have turbulent flow, which occurs only if the laminar flow is unstable. Therefore, it is important to analyze the stability of reacting shear layers; linear stability analysis is the most convenient tool for this purpose.

The stability of nonreacting mixing layers has been extensively investigated. In most of this work, analytic mean velocity profiles (usually hyperbolic tangent or error functions) were used. The validity of doing so needs investigation.

For incompressible parallel inviscid flow, Rayleigh[1] showed that, if the velocity profile has an inflection point, the flow is unstable. Lin[2] suggested that the inviscid mechanism dominates at large Reynolds numbers with viscosity producing only slight damping. Michalke[3] numerically integrated the Rayleigh stability equation with the hyperbolic-tangent velocity profile for temporally as well as spatially growing disturbances to incompressible flow; the spatial case results agreed well with experiments.

The effects of the mean velocity profile were studied by Monkewitz and Huerre,[4] who found that the amplification rate found with the Blasius mixing layer velocity profile agreed well with experimental results. Morkovin[5] suggested that only stability analyses based on mean profiles derived from the boundary-layer equations should be compared with experimental results; this is consistent with Michalke's proposition.

Koochesfahani and Frieler[6] investigated the linear spatial stability of plane mixing layers with both uniform and nonuniform density; they used analytical profiles. Kimura[7] constructed a stability theory for axisymmetric parallel flows and showed that the oscillation of laminar-jet flames can be explained by linear stability analysis. Trouve and Candel[8] did linear stability analysis of the inlet jet in a ramjet dump combustor using hyperbolic-tangent velocity and temperature profiles. They found that the density variation has a significant effect on the instability. Jackson and Grosch[9] studied the effect of heat release on the spatial stability of a supersonic reacting mixing layer using the hyperbolic-tangent velocity profile and the flame sheet approximation. Recently, Mahalingam et al.[10] studied the effects of heat release on the stability of coflowing, chemically reacting jets. They suggested that the heat release due to chemical reaction stabilized the flow.

For compressible flow, Groppengiesser[11] used laminar solutions of the compressible boundary-layer equations as the base flow and found a second mode of instability at high Mach number, which was subsequently rediscovered by Blumen et al.[12] Sandham and Reynolds[13] solved the linearized inviscid compressible stability equation and found maximum amplification at the frequency at which vortices are found in the laboratory. They also found that three-dimensional effects are important at high Mach number.

In this paper, we consider a low-speed, plane mixing layer in which fuel and oxidizer are initially unmixed. Laminar profiles obtained by solving the boundary-layer equations are used as input to linear stability analysis. The effects of heat release in both the laminar flow and the instability are studied as are the effects of variable transport properties. Both temporally and spatially developing layers are considered; the former are easier to understand, and the latter are used for comparison with experimental results.

II. Laminar Flow Profiles

To generate mean profiles, we solved the (parabolic) two-dimensional boundary-layer equations in the low Mach number approximation.[10,14] The effects of density variation, which can be quite large if the heating caused by chemical reaction is large, must be retained. The governing equations are given in the Appendix. All dependent variables are nondimensionalized using the values on the high-speed side. Uniform pressure through the shear layer and unity Lewis and Prandtl numbers are assumed for simplicity. We found that a Prandtl number of 0.7 does not produce large quantitative differences. Both freestreams are at the same temperature. The inlet profiles are taken from self-similar solutions of the equations for the time developing flow at low heat release but the temperature is arbitrarily increased so that reaction will proceed. Chemistry is represented by a single step irreversible scheme, involving fuel F and oxydizer O, reacting to yield a product P:

$$\nu_F F + \nu_O O \rightarrow \nu_P P \tag{1}$$

Presented as Paper 90-0268 at the AIAA 28th Aerospace Sciences Meeting, Reno, NV, Jan. 8-11, 1990; received April 9, 1990; revision received Dec. 4, 1990; accepted for publication Dec. 10, 1990.

*Research Assistant, Thermosciences Division, Department of Mechanical Engineering.

†Professor, Thermosciences Division, Department of Mechanical Engineering. Member AIAA.

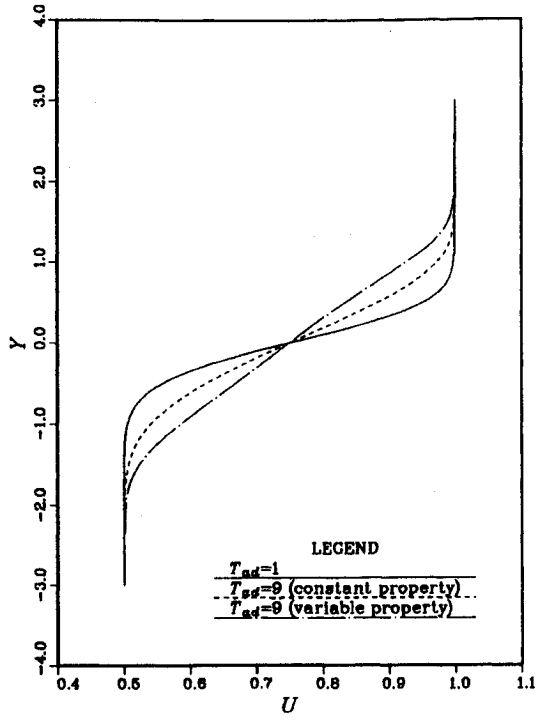

a)

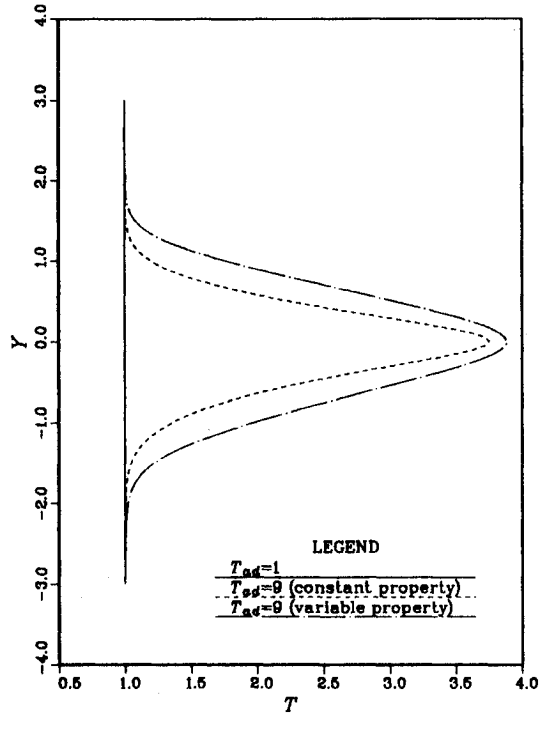

b)

Fig. 1 Effect of heat release and variable transport properties of the spatially developing layer for T_{ad} = 9: a) velocity; b) temperature.

where ν_F, ν_O, and ν_P are the stoichiometric coefficients for fuel, oxidizer, and product, respectively. Both constant and variable property cases are simulated. For the variable properties, power laws in temperature and pressure are assumed:

$$\mu \propto P^0 T^{0.7}, \qquad \kappa \propto P^0 T^{0.7}, \qquad D \propto P^1 T^{1.7} \tag{2}$$

where μ is the viscosity, κ the thermal diffusivity, and D the mass diffusivity. To satisfy the boundary-layer approximation, we used an initial Reynolds number of 1×10^3 based on the vorticity thickness and the cold viscosity. To include coupling between chemical reaction, heat release, and the velocity field, the continuity, momentum, energy, and species equations are solved simultaneously. As the boundary-layer equations are parabolic, an implicit method (Crank-Nicolson) is used. In the spatial layer, the correct boundary condition for the normal velocity V as $y \to \pm\infty$ is difficult to determine. We used the integral relation derived from the y-momentum equation:

$$\frac{d}{dx}\int_{-\infty}^{\infty} \rho UV \, dy + \rho_\infty V_\infty^2 - \rho_{-\infty} V_{-\infty}^2 = 0 \tag{3}$$

where ρ is the density and U the streamwise velocity. Tzuoo et al.[15] used this boundary condition for the incompressible case.

The magnitude of the normal velocity is <1% of the streamwise velocity in all computed profiles; this validates the use of the boundary-layer approximation.

Figures 1 compare the streamwise velocity and temperature profiles of the spatial layer for the same inlet profile and shows the effects of heat release and variable properties on the laminar flow. These profiles are compared at the same nondimensional streamwise distance x for downstream from the ignition point. The nondimensional adiabatic flame temperature T_{ad} is 9 for the reacting cases and the corresponding maximum temperatures are 4.55 for constant properties and 4.57 for variable properties, respectively. Figure 2 shows that the vorticity thickness δ_w with variable properties grows more rapidly as the adiabatic flame temperature increases. The significant difference between the constant and variable property solutions indicates that property variations need to be included whenever there are large temperature variations.

Figure 3 compares the laminar solution with a hyperbolic-tangent profile of the same vorticity thickness. The profile obtained from the simulation is fuller than the hyperbolic-tangent profile and, as we shall see, has very different stability properties.

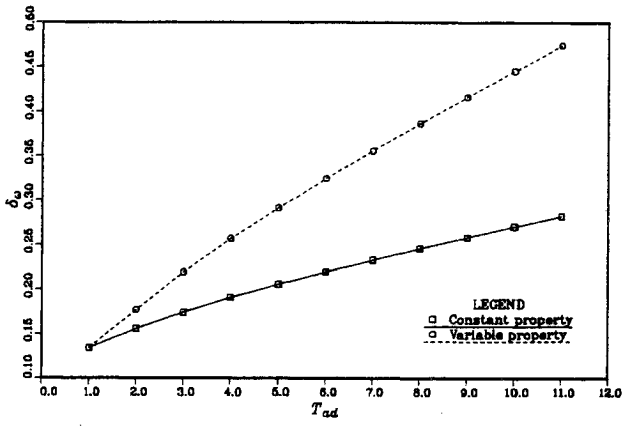

Fig. 2 Effect of heat release to the growth of the velocity thickness of spatially developing layer.

III. Linear Stability Analysis

A. Inviscid Linear Stability Equation

In linear inviscid stability analysis, all flow variables are assumed to be the sum of the mean and small wave-like fluctuations. The parallel flow assumption is made for the mean flow, which means that the predominant variation of the mean flow properties vary in the direction normal to the flow. All flow variables can be represented in the form:

$$f(x,y,z,t) = \bar{f}(y) + f'(x,y,z,t) \tag{4}$$

The disturbances represented by the primed variables are assumed to have the form of traveling waves:

$$f'(x,y,z,t) = \hat{f}(y) \exp[i(\alpha x + \beta z - \omega t)] \tag{5}$$

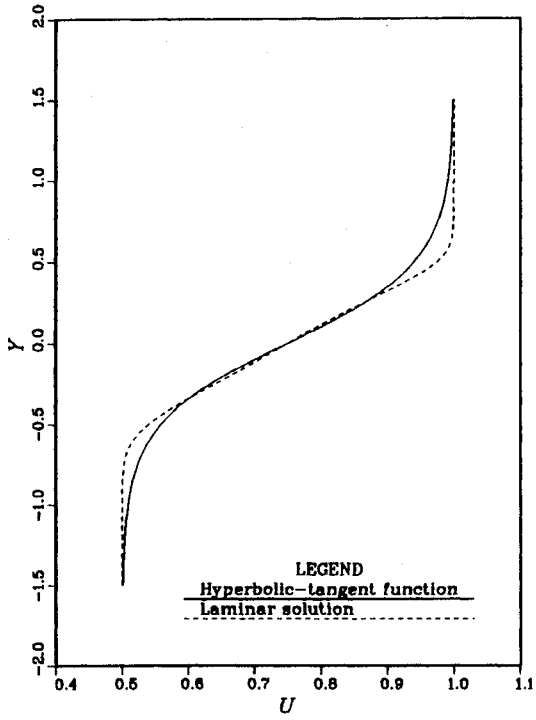

Fig. 3 Comparison of the hyperbolic-tangent and laminar solution velocity profiles for the spatially developing layer at $T_{ad} = 9$.

where $\hat{f}$ is an eigenfunction assumed to be a function of y only, α and β are wave numbers in the streamwise and spanwise directions, respectively, and ω is the frequency. The relation between the wave numbers and the angle of disturbance is

$$\tan\theta = \beta/\alpha \tag{6}$$

For the temporal stability analysis, α is real and ω is complex, whereas for the spatial analysis, ω is real and α is complex. The amplification rates for the two cases are ω_i and $-\alpha_i$, respectively.

The perturbation equations are derived by linearizing the low Mach number equations without using the boundary-layer approximations. Substituting Eq. (4) into these equations and neglecting the products of disturbances yields the equations for the perturbations. From the continuity and momentum equations, a disturbance equation for the pressure is obtained:

$$\hat{p}'' - \frac{2\alpha U'}{(\alpha U - \omega)}\hat{p}' + \hat{\rho}(\alpha U - \omega)^2 - (\alpha^2 + \beta^2)\hat{p} = 0 \tag{7}$$

where U is the mean velocity and a prime denotes differentiation with respect to y. This is the three-dimensional equation; for $\beta = 0$, it reduces to the two-dimensional one. Equation (7) reduces to the incompressible Rayleigh equation[16] if density is constant, i.e., $\hat{\rho} = 0$. Finally, $\hat{\rho}$ can be eliminated in favor of the mean pressure $\hat{p}$ using the state, energy, and species equations. Equation (7) then becomes

$$\hat{p}'' - \left\{\frac{2\alpha U'}{(\alpha U - \omega)} + \frac{R}{T}(\alpha U - \omega)^2[RXN]\right\}\hat{p}' - (\alpha^2 + \beta^2)\hat{p} = 0 \tag{8}$$

where R and T are the mean density and temperature, respectively. $[RXN]$ is a term that represents the effect of density variation due to chemical reaction and associated heat release; it is given in the Appendix. The boundary conditions are obtained by considering the asymptotic form of the solutions of Eq. (8). As $y \to \pm\infty$, U' and $[RXN]$ become negligible and the bounded solutions behave like

$$\hat{p}(y \to -\infty) = C_1 \exp(\sqrt{\alpha^2 + \beta^2}\,y) \tag{9a}$$

$$\hat{p}(y \to \infty) = C_2 \exp(-\sqrt{\alpha^2 + \beta^2}\,y) \tag{9b}$$

where C_1 and C_2 are arbitrary constants. A combination of the shooting and Newton-Raphson methods are used to solve Eq. (8). This method is applicable to both the temporal and spatial problems. Any velocity and temperature profiles can be specified as input to the stability calculation; in particular, either analytic functions or the computed laminar profiles can be used.

To confirm the validity of our equations and numerical methods, the incompressible case without chemical reaction (the Rayleigh problem) and the reacting flow with a hyperbolic tangent as its mean profile are examined. The results for the nonreacting case are compared with Michalke's[3] results in Fig. 4; the agreement is excellent. For the reacting flow, we compared our calculation with those of Trouve and Candel.[8] They used hyperbolic-tangent mean velocity and tem-

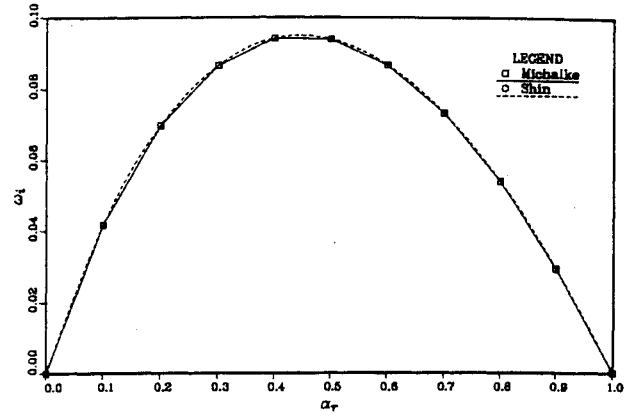

Fig. 4 Temporal growth rate in the incompressible case.

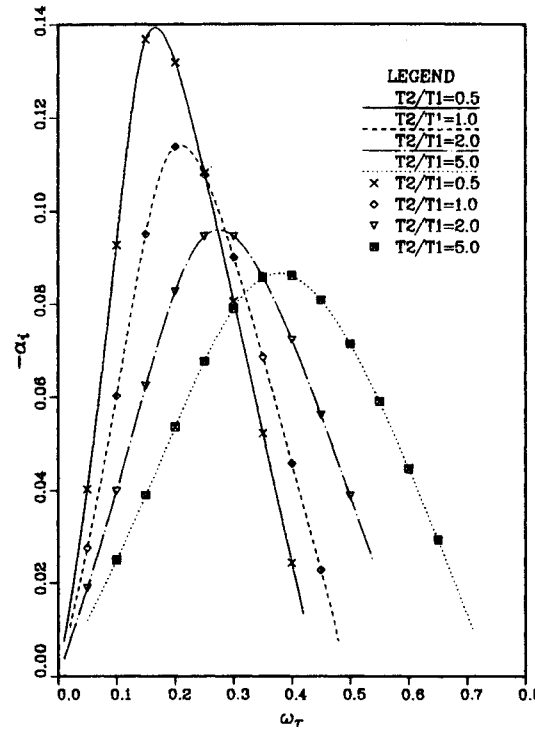

Fig. 5 Spatial growth rate of the mixing layer with mean profiles $U(y) = 1 + \tanh(y/2)$ and $T(y) = 1 + \lambda_t \tanh(y/2)$ (lines: Shin and Ferziger, current study; symbols: Trouve and Candel[8])

perature profiles,

$$U(y) = 1 + \tanh(y/2)$$
$$T(y) = 1 + \lambda_t \tanh(y/2)$$

where λ_t is the parameter for temperature ratio of two freestreams. Figure 5 shows the comparison between our calculation and Trouve and Candel's. Here, T_1 and T_2 are upper and lower freestream temperatures, respectively. Again, excellent agreement is obtained.

B. Inflection Points

According to Rayleigh's inflection-point theorem,[16] a necessary condition for instability is that the laminar velocity profile has an inflection point. For incompressible flow, this condition requires U'' to change sign at least once in the flow domain. A stronger form of this condition was obtained by Fjørtoft,[16] who proved that a necessary condition for instability is that $U''(U - U_s) < 0$ somewhere in the field, where y_s is a point at which $U'' = 0$ and $U_s = U(y_s)$. In this section, we generalize these theorems to flows that have density variation.

If we write the disturbance equation in terms of the normal fluctuating velocity $\hat{v}$, then, in temporal flow, the disturbance equation becomes

$$\left(\frac{\hat{v}'}{R}\right)' - \left\{\frac{(RU')'}{R^2(U - C)} + \frac{\alpha^2}{R}\right\}\hat{v} = 0 \qquad (10)$$

where C is the complex wave velocity. Multiplying this equation by $\hat{v}^*$, integrating from $-\infty$ to ∞, and integrating the first term by parts, we obtain

$$\int_{-\infty}^{\infty}\left\{\frac{|D\hat{v}|^2 + \alpha^2|\hat{v}|^2}{R} + \frac{(U - C_r)(RU')|\hat{v}|^2}{R^2|U - C|^2}\right\} + iC_i\int_{-\infty}^{\infty}\frac{(RU')'|\hat{v}|^2}{R^2|U - C|^2}\,dy = 0 \qquad (11)$$

where D is the differential operator d/dy, and C_r and C_i are the real and imaginary parts of the wave velocity, respectively. The imaginary part of Eq. (10) is

$$C_i\int_{-\infty}^{\infty}\frac{(RU')'|\hat{v}|^2}{R^2|U - C|^2}\,dy = 0 \qquad (12)$$

which can be satisfied only if $(RU')'$ changes sign at least once in the open domain $(-\infty,\infty)$; this is a necessary condition for instability. A stronger form of this condition can be obtained by considering the real part of Eq. (11):

$$\int_{-\infty}^{\infty}\frac{(U - C_r)(RU')'|\hat{v}|^2}{R^2|U - C|^2}dy = -\int_{-\infty}^{\infty}\frac{|D\hat{v}|^2 + \alpha^2|\hat{v}|^2}{R}dy \qquad (13)$$

Supposing that $C_i > 0$, multiplying Eq. (12) by $(C_r - U_s)/C_i$ and adding it to Eq. (13), we have

$$\int_{-\infty}^{\infty}\frac{(U - U_s)(RU')'|\hat{v}|^2}{R^2|U - C|^2}dy = -\int_{-\infty}^{\infty}\frac{|D\hat{v}|^2 + \alpha^2|\hat{v}|^2}{R}dy \qquad (14)$$

Thus, a necessary condition for instability is $(RU')'(U - U_s) < 0$ somewhere on the domain $-\infty < y < \infty$. The mean profiles were searched for points that satisfy this condition. Figure 6a shows that the cold flow has just one inflection point, whereas the reacting flow has three. Figure 6b shows a test of the strong necessary condition for instability. All three inflection points satisfy the necessary condition. The reacting mixing layer should, therefore, be unstable to three distinct modes.

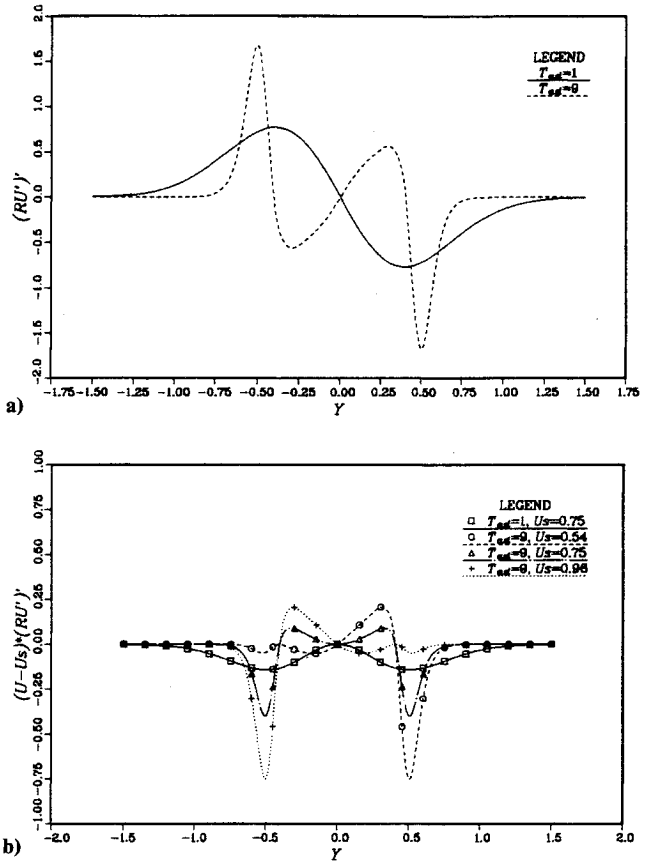

Fig. 6 Function appearing in the necessary condition for temporal instability: a) $(RU')'$; b) $(RU')'(U - U_s)$.

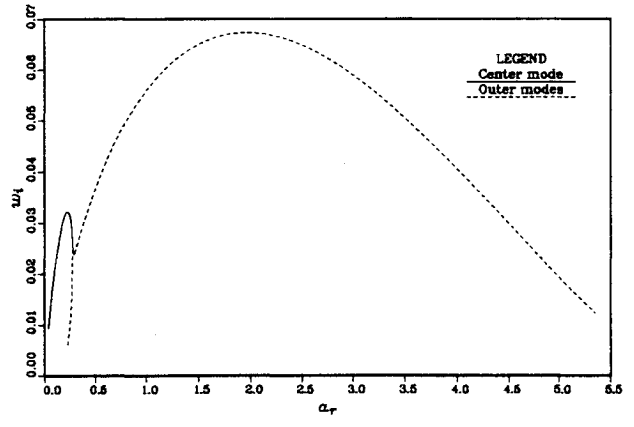

Fig. 7a Growth rate of the multiple instability modes in the temporal flow at $T_{ad} = 9$.

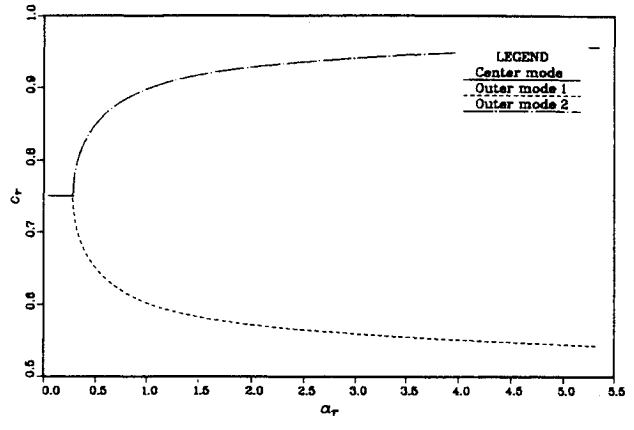

Fig. 7b Phase velocity.

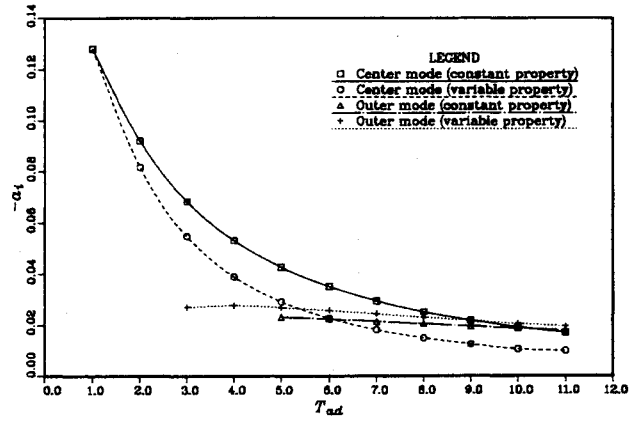

Fig. 8 Effect of heat release on the amplification rate (spatial instability).

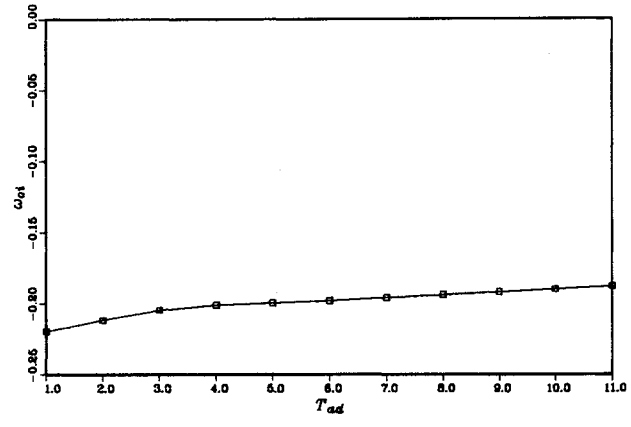

Fig. 9 Variation of ω_{oi} with adiabatic flame temperature (spatial instability).

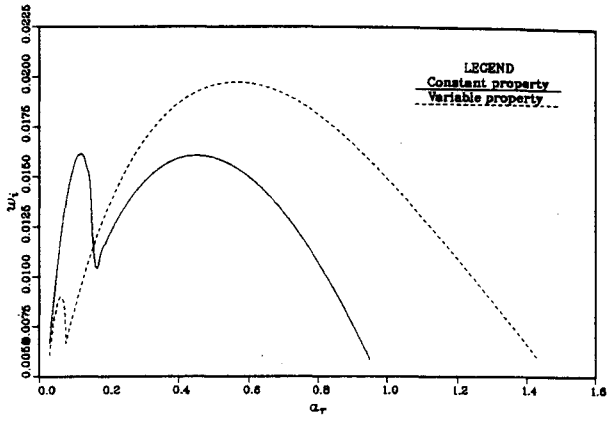

Fig. 10 Effect of variation of properties on the growth rate at T_{ad} = 9 (temporal instability).

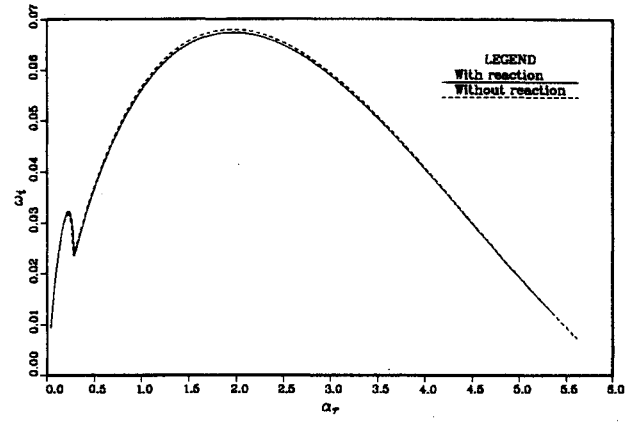

Fig. 11 Effect of reaction during instability on the growth rate at T_{ad} = 9 (temporal instability).

C. Multiple Modes of Instability

In the last section, we showed that the mean profiles for reacting flow have three inflection points and should have three independent modes of instability. In the temporal stability case, symmetry dictates that two of these be reflections of each other. Figures 7 show the amplification rate and phase velocity as a function of the wave number for a variable property flow with T_{ad} = 9. For the amplification rate, only two modes are shown. The first is the center mode that arises from the central inflection point; its phase velocity is the mean velocity at the central inflection point. The second represents both of the modes due to the outer inflection points. The phase velocities of the two outer modes are different, as shown in Fig. 7b, and they approach the mean velocities at the outer inflection points as the wave number increases.

The center mode travels at the same phase velocity as in the cold flow, the average of the two freestream velocities. One of the outer modes travels at lower speed than the center mode, whereas the other travels at higher speed. Similar results were found in compressible flow by Sandham.[17]

We shall show in the next section that, for large heat release, the outer modes are more amplified and should dominate. These modes are also very sensitive to the variation of the properties, and so the latter is very important in this flow.

D. Effect of Heat Release, Variable Properties, and Reaction

Figure 8 shows the effect of heat release on the maximum growth rate for the spatially developing layer; computed laminar profiles were used in these calculations. As the heat release increases, the maximum amplification rate of the center mode decreases. The maximum amplification rate in the cold flow is 0.128, but for the variable property case with T_{ad} = 10, it is 0.01, or only 8% that of the cold flow. On the other hand, the amplification rate of the outer mode changes very little as the heat release increases. Consequently, at high heat release, the outer mode is more amplified than the center mode. When T_{ad} is 10, the outer mode has almost three times the amplification rate of the center mode. Thus, reacting flows with high heat release should be unstable to the short wavelength outer modes.

The absolute and convective instability of the spatially developing layer are distinguished by the temporal growth rate, which is positive in the absolute and negative in the convective case, of the mode that dominates the response at the source location. In physical terms, in absolute instability, a locally generated small amplitude transient grows exponentially in time, whereas in convective instability, transient is convected away and leaves the mean flow ultimately undisturbed. Huerre and Monkewitz[18] showed that a flow is convectively unstable if the modes that have zero group velocity are temporally damped, i.e., the imaginary parts of the complex frequencies are negative and absolutely unstable if all are positive. We used this criterion to determine the nature of the instability of the reacting mixing layer. First, we found the complex frequency ω_o, which makes the group velocity $d\omega/d\alpha$ zero. The imaginary part of this frequency ω_{oi} is the absolute growth rate that determines the nature of the instability. Figure 9 shows the imaginary part of ω_o as a function of the adiabatic flame temperature T_{ad}. All ω_{oi} are negative, and, therefore, the reacting mixing layers considered here are convectively unstable.

In Sec. II, we showed that the variation of the properties through the reacting shear layer influences the mean flow profiles significantly. Figure 10 shows that that effect results in the difference in stability characteristics when T_{ad} = 9. The constant property case has twice the growth rate of the center mode of the variable property case; however, the latter has the growth rates of the outer modes, which are almost 25%

higher. The constant property profile has the center and outer modes with comparable amplification rates, but for the variable property profile, the outer modes are dominant over the center mode. Again, the importance of the variable properties is emphasized.

The density variation in the laminar flow is much more important than chemical reaction that occurs during the instability. Figure 11 shows that including the chemical reaction terms in the instability calculation hardly changes the amplification rate, a result in agreement with one of Mahalingam et al.[19] These results suggest that, in the linear stability analysis, chemical reaction can be ignored.

Squire's transformation[16] allows the three-dimensional Rayleigh problem to be reduced to the two-dimensional problem. One can then show that two-dimensional modes dominate in incompressible flow. In compressible flow, the reduction to a two-dimensional problem is no longer possible and the obliquity of the most amplified wave increases with Mach number.[13] We want to determine whether Squire's transformation can be applied to the reduction of the problem with heat release. If we discard the chemical reaction during the instability, use Eq. (6), and let

$$\tilde{\alpha} = (\alpha^2 + \beta^2)^{1/2}, \qquad \tilde{p}/\tilde{\alpha} = \hat{p}/\alpha, \qquad \tilde{\omega}/\tilde{\alpha} = \omega/\alpha \tag{15}$$

then Eq. (8) becomes

$$\tilde{p}'' - \left\{\frac{2\tilde{\alpha}U'}{(\tilde{\alpha}U - \tilde{\omega})} + \frac{T'}{T}\right\}\tilde{p}' - \tilde{\alpha}^2\tilde{p} = 0 \tag{16}$$

Equation (16) is exactly the two-dimensional version of Eq. (8) if the chemical reaction is neglected in the stability analysis. Thus, provided the chemical reaction is neglected, Squire's transformation does reduce the three-dimensional problem to an equivalent two-dimensional problem. Two-dimensional modes are more amplified than three-dimensional ones. Three dimensionality is not important even though there is density variation due to heat release.

E. Mean Flow

In this section, the validity of using analytical flow profiles such as hyperbolic-tangent and error functions is investigated. To accomplish this goal, we compare results obtained from these profiles with ones based on the boundary-layer solutions.

The analytical profiles also have three different modes. Figures 12 show the amplification rates vs wave number. In Fig. 12a, results for temporal layers are given. For the center mode, the differences are small, but for the outer mode, the growth rate obtained from the laminar solution is about twice that obtained with the error function. This is not surprising since the principal differences in the profiles are found in the outer parts of the layers. In Fig. 12b, the hyperbolic-tangent function results are compared with the laminar solution for the spatial layer. Again, there is little difference for the center mode, but for the outer mode, the hyperbolic-tangent function has a lower growth rate than the laminar solution. From these results, we find that the use of accurate laminar profiles is essential. This is consistent with the report by Monkewitz and Huerre.[4]

F. Linear Eigenfunctions and Vorticity Distribution

The eigenfunctions of the linear stability problem provide information about the large-scale motions that result from the linear instability. From these eigenfunctions and the mean flow, a qualitative approximation to a typical flow variable f can be calculated for one wavelength in the x direction:

$$f = \bar{f} + a\mathcal{R}[\hat{f}e^{i\alpha x}] \tag{17}$$

where $\mathcal{R}$ denotes the real part of the fluctuating part of a flow

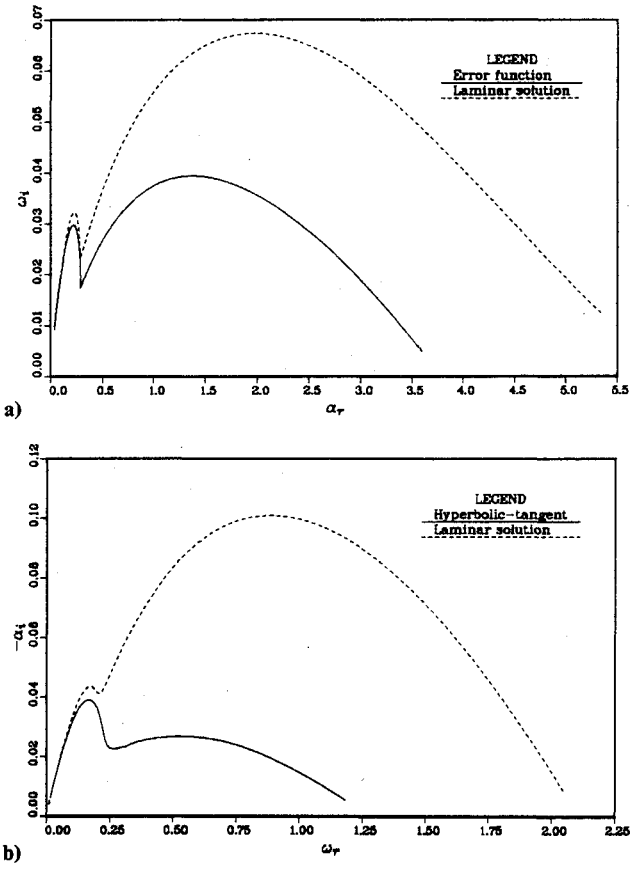

Fig. 12 Effect of velocity profiles on linear growth rate at T_{ad} = 9: a) temporal instability; b) spatial instability.

variable. The amplitude of the disturbance a was chosen as 0.4 to emphasize the structure. From the eigenfunctions and the mean flow, disturbance vorticity and total vorticity distributions can be obtained.

In Figs. 13a–e, the total vorticity contours are plotted for the cold flow and the reacting flow for T_{ad} = 9. The vorticity structure for the cold flow (Fig. 13a) is identical to Michalke's.[3] The vorticity structure of the center mode for the reacting flow is quite different from the cold flow structure. There are four vorticity maxima in the heated flow, but only two in the cold flow; its wavelength is five times longer than the cold flow. The two outer modes have the same growth rates but different phase velocities. The low-speed mode has a vortex core below the center of the layer. The other mode is obtained by reflection. The wavelengths of these modes are half of the cold flow wavelength. In each case, the vorticity maxima are expected to roll up into large structures similar to the ones found in the cold flow.

Large spanwise vortices were identified by Winant and Browand[20] and Brown and Roshko[21] as the principal features of two-dimensional mixing layers in the region following the linear domain, but preceding the establishment of fully turbulent flow conditions. The initial vortex spacings are related to the initial wavelength of the instability. Hermanson and Dimotakis[22] reported that the vortex spacing in a reacting shear layer decreased as much as 25% relative to the cold flow for a mean density reduction of 40%. According to our calculations with the same mean density reduction, the initial wavelength of the outer mode decreases by about 40%, whereas the center mode wavelength increases 400%. Thus, there is just a small quantitative difference between our predictions and their experiments. This might be due to different Reynolds numbers and/or initial profiles. We take this as evidence that the outer mode is dominant in their flow and that the agreement is reasonable.

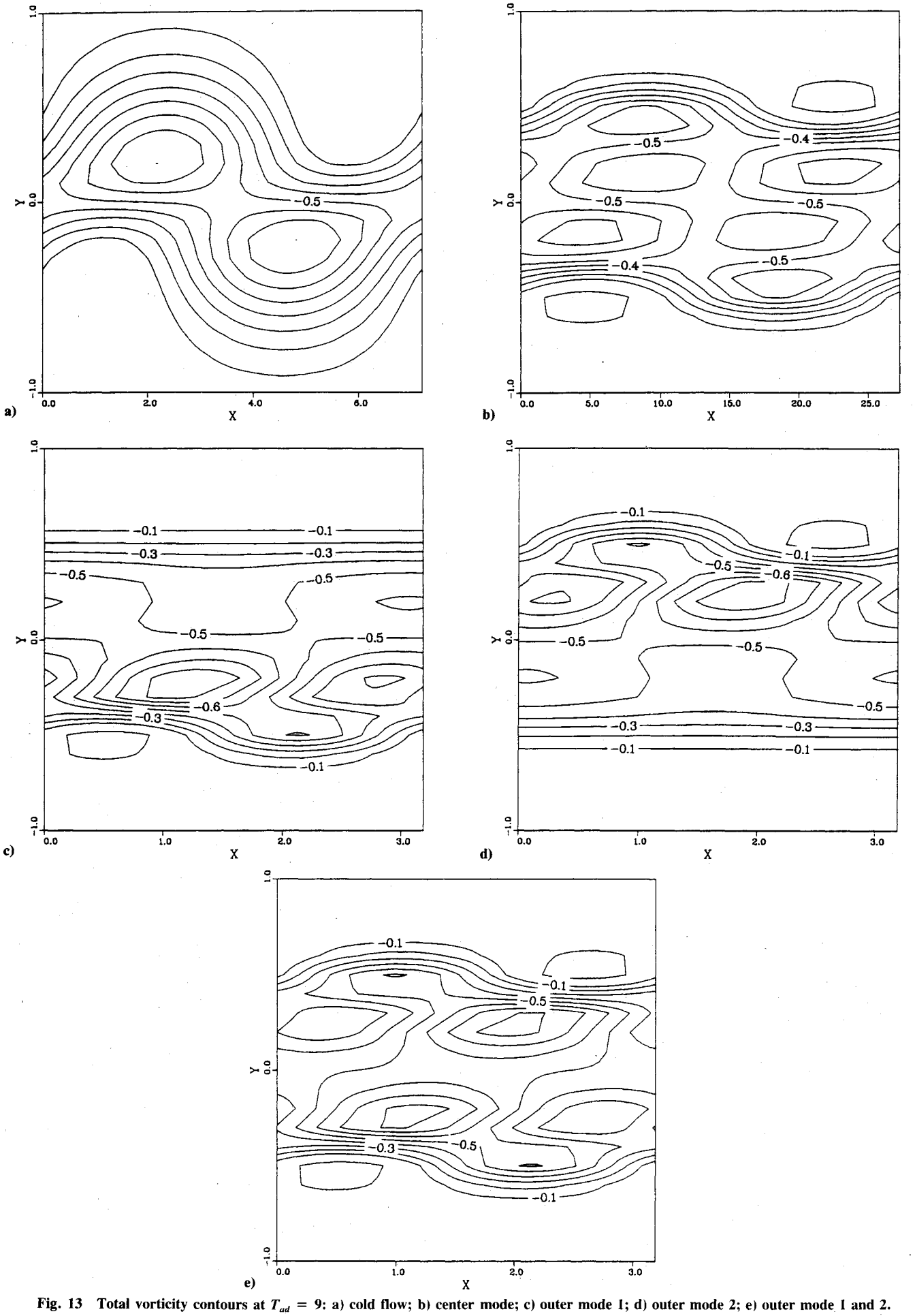

Fig. 13 Total vorticity contours at $T_{ad} = 9$: a) cold flow; b) center mode; c) outer mode 1; d) outer mode 2; e) outer mode 1 and 2.

The linear eigenfunctions can also provide initial conditions for direct numerical simulations. We expect to do two-dimensional direct numerical simulations to confirm the results of the linear stability study and to see the effects of the heat release to the later development of the plane mixing layer.

IV. Conclusions

We have shown that stability of reacting flows can be studied by linear stability analysis. The growth rates are very sensitive to the mean profiles. Boundary-layer equation solutions obtained with variable transport properties are more realistic representations of an actual flow than analytically prescribed functions and thus provide a better basis for stability analysis.

For the reacting plane mixing layer with variable density, a necessary condition for instability has been derived. New inflectional modes of instability are found to exist in the outer part of the mixing layer. Heat release stabilizes the flow and, in particular, greatly reduces the growth rate of the center mode. The outer modes, which do not exist for $T_{ad} < 3$, have growth rates that are relatively insensitive to heat release for $T_{ad} > 5$. For the large heat releases typical of combusting flows, the outer mode is more amplified than the center mode; its wavelength is about one-tenth that of the center mode. The density variation caused by chemical reaction in the laminar flow has a much larger effect on the growth rate of the instability than chemical reaction during the instability. Unlike the compressible plane mixing layer, even at high heat release, two-dimensional waves are more amplified than three-dimensional ones.

From the eigensolutions of the linear theory, information about the vortex structure of the flow that develops from the instability can be obtained. Both the outer and the center modes have four large vorticity concentrations per wavelength; these are expected to develop into large-scale structures.

Appendix

Two-Dimensional Boundary-Layer Equations for Mean Flow

Continuity equation:

$$\frac{\partial \rho}{\partial t} + \frac{\partial \rho u}{\partial x} + \frac{\partial \rho v}{\partial y} = 0$$

Momentum equation:

$$\frac{\partial \rho u}{\partial t} + \frac{\partial \rho u^2}{\partial x} + \frac{\partial \rho v u}{\partial y} = \frac{1}{Re}\frac{\partial}{\partial y}\left(\mu \frac{\partial u}{\partial y}\right)$$

Energy equation:

$$\frac{\partial \rho T}{\partial t} + \frac{\partial \rho u T}{\partial x} + \frac{\partial \rho v T}{\partial y} = \frac{1}{PrRe}\frac{\partial}{\partial y}\left(\kappa \frac{\partial T}{\partial y}\right) + Da\, w_T$$

Species equation:

$$\frac{\partial \rho y_i}{\partial t} + \frac{\partial \rho u y_i}{\partial x} + \frac{\partial \rho v y_i}{\partial y} = \frac{1}{PrPe}\frac{\partial}{\partial y}\left(\rho D \frac{\partial y_i}{\partial y}\right) + Da\, w_i$$

State equation:

$$P = \rho T$$

The dependent variables are in nondimensional form. The symbols ρ, u, v, T, and P represent the density, velocities in x, y direction, temperature, and pressure, respectively. The y_F, y_O, and y_P represent the mass fractions of fuel, oxidizer, and product species, respectively. Henceforth, the subscript i stands for any of the species. W_i, ν_i', and ν_i'' represent, respectively, the molecular weight and the stoichiometric coefficient of species when appearing as a reactant and or a product. [Thus, ν_O' is ν_O, whereas ν_O'' is zero for the scheme in Eq. (1).] The ω_T and ω_i are the rate of heat release and the reaction rate of species i, respectively, and they are defined as follows:

$$\omega_T = \frac{Q}{W_F \nu_F}(\rho y_F)(\rho y_O)\exp\left[-\beta'\left(\frac{1}{T} - 1\right)\right]$$

$$\omega_i = \frac{W_i(\nu_i'' - \nu_i')}{W_F \nu_F}(\rho y_F)(\rho y_O)\exp\left[-\beta'\left(\frac{1}{T} - 1\right)\right]$$

The nondimensional heat of reaction Q expressed in terms of dimensional variables is

$$Q = \frac{[h_F^0 W_F \nu_F + h_O^0 W_O \nu_O - h_P^0 W_P \nu_P]}{C_P T_{\text{ref}}}$$

where h_i^0 represents the enthalpy of formation of species i, C_P is the specific heat at constant pressure, and T_{ref} is the reference temperature. Re, Pr, Pe, and Da are Reynolds number, Prandtl number, Peclet number, and Damköhler number, respectively. β' is a nondimensional activation energy parameter.

Representation of [RXN]

The term $[RXN]$ of Eq. (8) may be written as a ratio of determinants:

$$[RXN] = \frac{\begin{vmatrix} A & B & C \\ D & E & F \\ G & H & I \end{vmatrix}}{\begin{vmatrix} A & B & J \\ D & E & K \\ G & H & L \end{vmatrix}}$$

The elements of these determinants are

$$A = iR(\alpha U - \beta) + DaR^2 Y_O \exp\left[-\beta'\left(\frac{1}{T} - 1\right)\right]$$

$$B = DaR^2 Y_F \exp\left[-\beta'\left(\frac{1}{T} - 1\right)\right]$$

$$C = \frac{-iY_F'}{(\alpha U - \beta)}$$

$$D = Da\frac{W_O \nu_O}{W_F \nu_F} R^2 Y_O \exp\left[-\beta'\left(\frac{1}{T} - 1\right)\right]$$

$$E = iR(\alpha U - \beta) + Da\frac{W_O \nu_O}{W_F \nu_F} R^2 Y_O \exp\left[-\beta'\left(\frac{1}{T} - 1\right)\right]$$

$$F = \frac{-iY_O'}{(\alpha U - \beta)}$$

$$G = Da\frac{Q}{W_F \nu_F} R^2 Y_O \exp\left[-\beta'\left(\frac{1}{T} - 1\right)\right]$$

$$H = Da\frac{Q}{W_F \nu_F} R^2 Y_F \exp\left[-\beta'\left(\frac{1}{T} - 1\right)\right]$$

$$I = \frac{-iT'}{(\alpha U - \beta)}$$

$$J = -Da\left[2\frac{R^2}{T}Y_FY_O - \frac{R^2}{T^2}Y_FY_O\beta'\right]\exp\left[-\beta'\left(\frac{1}{T}-1\right)\right]$$

$$K = -Da\frac{W_O\nu_O}{W_F\nu_F}\left[2\frac{R^2}{T}Y_FY_O - \frac{R^2}{T^2}Y_FY_O\beta'\right]\exp\left[-\beta'\left(\frac{1}{T}-1\right)\right]$$

$$L = iR(\alpha U - \beta) + Da\frac{Q}{W_F\nu_F}\left[2\frac{R^2}{T}Y_FY_O - \frac{R^2}{T^2}Y_FY_O\beta'\right]\exp\left[-\beta'\left(\frac{1}{T}-1\right)\right]$$

where the quantities Y_F, Y_O represent the mean fuel and oxidizer species profiles, respectively.

Acknowledgment

This work was sponsored by NASA Ames Research Center under Contract NASA NCA2-285.

References

[1]Rayleigh, Lord, "On the Stability, or Instability, of Certain Flow Motions," *Proceedings of the London Math. Soc.* Vol. 11, 1880, pp. 57–70.

[2]Lin, C. C., *The Theory of Hydrodynamic Stability*, Cambridge Univ. Press, Cambridge, England, UK, 1955.

[3]Michalke, A., "On the Inviscid Instability of the Hyperbolic-Tangent Velocity Profile," *Journal of Fluid Mechanics*, Vol. 19, Aug. 1964, pp. 543–556.

[4]Monkewitz, P. A., and Huerre, P., "Influence of the Velocity Ratio on the Spatial Instability of Mixing Layers," *Physics of Fluids*, Vol. 25, July 1982, pp. 1137–1143.

[5]Morkovin, M. V., "Guide to Experiments on Instability and Laminar-Turbulent Transition in Shear Layers," NASA Ames short course, 1988.

[6]Koochesfahani, M. M., and Frieler, C. E., "Inviscid Instability Characteristics of Free Shear Layers with Non-Uniform Density," AIAA Paper 87-0047, Jan. 1987.

[7]Kimura, I., "Stability of Laminar Jet Flames," *Tenth Symposium (International) on Combustion*, The Combustion Inst., Pittsburgh, PA, 1965, pp. 1295–1300.

[8]Trouve, A., and Candel, S. M., "Linear Stability of the Inlet Jet in Ramjet Dump Combustor," AIAA Paper 88-0149, Jan. 1988.

[9]Jackson, T. L., and Grosch, C. E., "Effect of Heat Release on the Spatial Stability of a Supersonic Reacting Mixing Layer," NASA CR-181753, Nov. 1988.

[10]Mahalingam, S., Cantwell, B., and Ferziger, J., "Effects of Heat Release on the Structure and Stability of a Coflowing, Chemically Reacting Jet," AIAA Paper 89-0691, Jan. 1989.

[11]Groppengiesser, H., "Study on the Stability of Boundary Layers in Compressible Fluids," NASA TT F-12, 786. Feb. 1970.

[12]Blumen, W., Drazin, P. G., and Billings, D. F., "Shear Layer Instability of an Inviscid Compressible Fluid. Part 2," *Journal of Fluid Mechanics*, Vol. 71, Sept. 1975, pp. 305–316.

[13]Sandham, N., and Reynolds, W., "The Compressible Mixing Layer: Linear Theory and Direct Simulation," AIAA Paper 89-0371, Jan. 1989.

[14]McMurtry, P. A., Jou, W. H., Riley, J. J., and Metcalfe, R. W., "Direct Numerical Simulations of a Reacting Mixing Layer with Chemical Heat Release," AIAA Paper 85-0143, 1985.

[15]Tzuoo, K. S., Ferziger, J. H., and Kline, S. J., "Zonal Models of Turbulence and Their Application to Free Shear Flows," Dept. of Mechanical Engineering, Stanford Univ., Stanford, CA, TF-27, Nov. 1986.

[16]Drazin, P. G., and Reid, W. H., *Hydrodynamic Stability*, Cambridge Univ. Press, Cambridge, England, UK, 1982, pp. 129–132.

[17]Sandham, N. D., and Reynolds, W. C., "A Numerical Investigation of the Compressible Mixing Layer," Dept. of Mechanical Engineering, Stanford Univ., Stanford, CA, TF-45, Sept. 1989.

[18]Huerre, P., and Monkewitz, P. A., "Absolute and Convective Instabilities in Free Shear Layers," *Journal of Fluid Mechanics*, Vol. 159, 1985, pp. 151–168.

[19]Mahalingam, S., Cantwell, B. J., and Ferziger, J. H., "Non-Premixed Combustion: Full Numerical Simulation of Coflowing Axisymmetric Jet, Inviscid and Viscous Stability Analysis," Dept. of Mechanical Engineering, Stanford Univ., Stanford, CA, TF-43, Aug. 1989.

[20]Winant, C. D., and Browand, F. K., "Vortex Paring: The Mechanism of Turbulent Mixing Layer Growth at Moderate Reynolds Number," *Journal of Fluid Mechanics*, Vol. 63, April 1974, pp. 237–255.

[21]Brown, G. L., and Roshko, A., "On Density Effects and Large Structures in Turbulent Mixing Layers," *Journal of Fluid Mechanics*, Vol. 64, July 1974, pp. 775–781.

[22]Hermanson, J. C., and Dimotakis, P. E., "Effects of Heat Release in a Turbulent, Reacting Shear Layer," *Journal of Fluid Mechanics*, Vol. 199, Feb. 1989, pp. 333–375.